Formation of an Electron-Phonon Bifluid in Bulk Antimony

Alexandre Jaoui,[1,2,*,†] Adrien Gourgout,[2] Gabriel Seyfarth,[3] Alaska Subedi,[4,5] Thomas Lorenz,[6] Benoît Fauqué,[1] and Kamran Behnia[2,‡]

[1]*JEIP, USR 3573 CNRS, Collège de France, PSL Research University, 11, Place Marcelin Berthelot, 75231 Paris Cedex 05, France*
[2]*Laboratoire de Physique et d'Étude des Matériaux (ESPCI—CNRS—Sorbonne Université), PSL Research University, 75005 Paris, France*
[3]*LNCMI-EMFL, CNRS, Université Grenoble Alpes, INSA-T, UPS, Grenoble, France*
[4]*CPHT, CNRS, Ecole Polytechnique, IP Paris, F-91128 Palaiseau, France*
[5]*Collège de France, 11 Place Marcelin Berthelot, 75005 Paris, France*
[6]*II. Physikalisches Institut, Universität zu Köln, 50937 Köln, Germany*

(Received 11 January 2022; revised 1 April 2022; accepted 7 June 2022; published 5 August 2022)

The flow of charge and entropy in solids usually depends on collisions decaying quasiparticle momentum. Hydrodynamic corrections can emerge, however, if most collisions among quasiparticles conserve momentum and the mean-free path approaches the sample dimensions. Here, through a study of electrical and thermal transport in antimony (Sb) crystals of various sizes, we document the emergence of a two-component fluid of electrons and phonons. Lattice thermal conductivity is dominated by electron scattering down to 0.1 K and displays prominent quantum oscillations. The Dingle mobility does not vary despite an order-of-magnitude change in transport mobility. The Bloch-Grüneisen behavior of electrical resistivity is suddenly aborted below 15 K and replaced by a quadratic temperature dependence. At the Kelvin temperature range, the phonon scattering time and the electron-electron scattering time display a similar amplitude and temperature dependence. Taken together, the results draw a consistent picture of a bifluid where frequent momentum-conserving collisions between electrons and phonons dominate the transport properties.

DOI: 10.1103/PhysRevX.12.031023 Subject Areas: Condensed Matter Physics

I. INTRODUCTION

Hydrodynamic corrections [1] to transport properties of solids can emerge when the traveling quasiparticle endures momentum-conserving collisions outweighing the momentum-relaxing ones. Their signatures are reported for electrons in mesoscopic metals [2–7] and for phonons in bulk insulators [8–11]. The possible role played by phonons in the emergence of hydrodynamic effects in the electronic fluid [12] has become a subject of recent theoretical attention [13–16]. It remains to be seen if momentum exchange between electron and phonon baths can generate experimental signatures other than phonon drag [17], the well-known nondiffusive thermoelectric response of heat-carrying phonons coupled to the electron bath [18].

Bulk semimetals are promising platforms for this investigation. Their small Fermi surface pockets imply reduced umklapp electron-electron scattering. Transport studies find that a significant fraction of electron-electron scattering conserves momentum in WP_2 [6,19] and in Sb [20], generating a downward departure from the Wiedemann-Franz (WF) law around $T \approx 10$ K, near the onset of the ballistic regime. Magnetic imaging experiments [14] find a Poiseuille profile of electron flow in the same temperature range in WTe_2. According to theoretical calculations, phonons play a prominent role in the emergence of this hydrodynamic window [14], a conjecture supported by Raman scattering experiments in WP_2 [21].

Here, we present direct evidence for phonon-electron coupling in bulk antimony. We find that the thermal diffusivity of phonons displays a nonmonotonic temperature dependence as observed in several other solids. In contrast to all other cases, however, instead of entering a ballistic regime upon further cooling, the phonons continue to exchange momentum with charge carriers down to 0.1 K. Thermal conductivity, phonon dominated by many orders of magnitude above 1 T, displays quantum oscillations.

*alexandre.jaoui@espci.fr
†Present address: Fakultät für Physik, Ludwig-Maximilians-Universität München, Geschwister-Scholl-Platz 1, 80539 München, Germany.
‡kamran.behnia@espci.fr

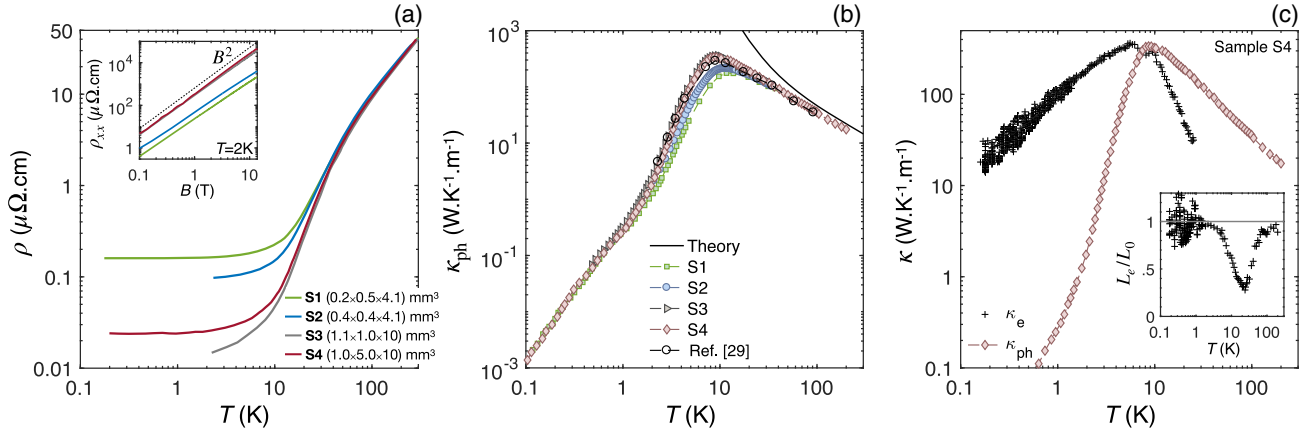

FIG. 1. Electrical and thermal conductivity in Sb crystals along the bisectrix crystallographic orientation. (a) Temperature dependence of the electrical resistivity ρ of four different Sb crystals with different sizes, as indicated in the legend. Residual resistivity is lowest in the largest samples. The inset shows the magnetoresistance of these crystals at $T = 2$ K. (b) Lattice thermal conductivity κ_{ph} of the same four Sb samples. Data from a previous report on a Sb rod [29] are also included. Note the absence of size dependence at low temperatures. The solid line represents theoretical lattice thermal conductivity considering only three-phonon scattering events (and neglecting scattering by electrons). Note that, at high temperature, theory tracks the experimental data but not at low temperature. We attribute this to significant scattering of phonons by electrons. (c) Temperature dependence of the electronic and phononic contributions to the total thermal conductivity in sample S4. The procedure for separation is discussed in detail in Supplemental Material [22]. The inset shows the temperature dependence of the electronic Lorenz number $L_e = \kappa_e \rho / T$ normalized by L_0, the Sommerfeld value.

The phononic viewpoint from thermal transport is complemented by the electronic viewpoint studied from electrical transport. As expected in the Bloch-Grüneisen picture of electron-phonon (e-ph) scattering, the exponent of resistivity increases when the system is cooled below the Debye temperature, but the steady enhancement is suddenly interrupted. Below $T \approx 15$ K, the electrical resistivity becomes purely T-square. We argue that this is because the smallness of phonon wave vector does not allow umklapp events, and, therefore, e-ph scattering does not contribute to resistivity. Around 1 K, the amplitude and the temperature dependence of the phonon scattering time (extracted from phonon conductivity) and the e-e scattering (extracted from electronic transport) match each other in amplitude and temperature dependence. The most plausible explanation for this is that colliding electrons exchange phonons as previously suspected [14].

Our scenario is backed by comparisons between the transport properties of antimony and metals with larger (i.e., copper or tungsten) and lower (bismuth or black phosphorous) carrier densities. There is roughly one charge carrier per 1000 atoms in antimony. The Fermi surface is small enough to push the mean-free path of electrons close to ballistic but also sufficiently large to render electrons capable of scattering phonons when phonon-phonon collisions cease to decay the heat current well below the Debye temperature.

II. RESULTS

Figure 1 shows the temperature dependence of electrical resistivity and thermal conductivity in antimony. As discussed in Supplemental Material [22], the electronic κ_e and the phononic κ_{ph} components of the total thermal conductivity κ can be easily separated thanks to the large sensitivity of κ_e to the magnetic field (a consequence of the huge magnetoresistance) and the field independence of κ_{ph}. As seen in Fig. 1(b), κ_{ph} peaks at $T \approx 10$ K and (in contrast to the strong size dependence of κ_e [20]) does not show any dependence on the sample size at low temperature. We discuss the implications of this feature below. This figure also shows the theoretical κ_{ph} computed from the phonon spectrum. The calculations neglect scattering by electrons, the finite sample size, and defects. They are also restricted to three-phonon scattering events. As seen in the figure, the experimental and the theoretical κ_{ph} are close to each other at room temperature. However, there is a deficit in the measured κ_{ph}, compared to the predicted one. The difference grows with cooling. Similar theoretical calculations yield a quantitative account of the experimental data down to low temperature in Si [23], GaAs [24], PbTe [25], SnSe [26], Al_2O_3 [27], and In_2O_3 [28]. Scattering of phonons by electrons is the most plausible reason that this is not the case of antimony.

In the vicinity of its peak, κ_{ph} depends on the sample size. This is more clearly seen in Fig. 2(a), which shows the temperature dependence of κ_{ph}/T^3 and its prominent peak. Figure 2(b) shows the lattice specific heat C_{ph} below 20 K. It does not follow a T^3 behavior but is in excellent agreement with our first-principle calculations of the phonon spectrum (see the details in Supplemental Material [22]). This agreement implies that the discrepancy between theoretical and experimental κ_{ph} is not a matter of

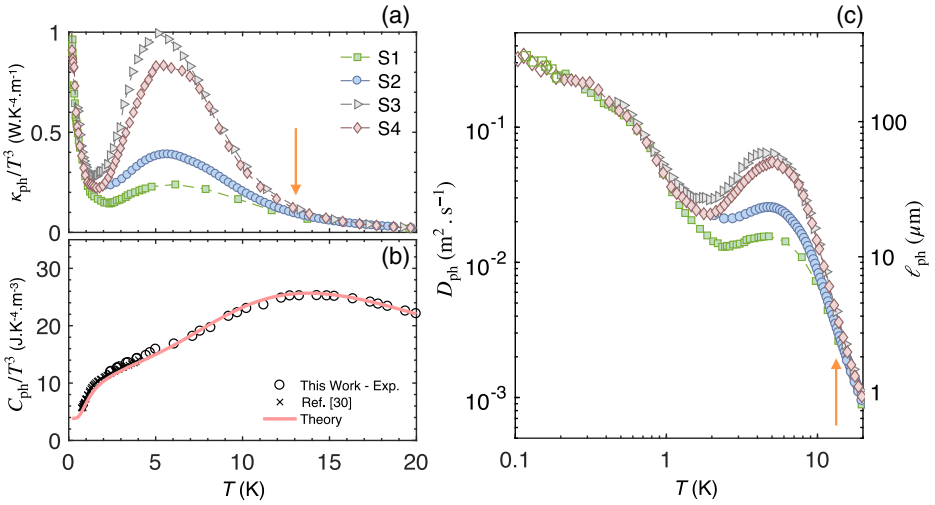

FIG. 2. Thermal conductivity, heat capacity, and thermal diffusivity of phonons. (a) Phononic thermal conductivity κ_{ph}, plotted as κ_{ph}/T^3 as a function of the temperature. (b) The phononic specific heat C_{ph} divided by T^3 together with a previous report [30]. The solid line represents *ab initio* calculations. (c) The lattice thermal diffusivity D_{ph} (left y axis) and phonon mean-free path ℓ_{ph} (right y axis) vs temperature. Note the emergence of a size-dependent peak and a minimum in the $T = 2$–15 K temperature range. Orange arrows indicate the temperature below which D_{ph} and κ_{ph} become size dependent.

the phonon spectrum but due to a scattering mechanism neglected by the theory.

One can extract the temperature dependence of phonon thermal diffusivity by combining the two sets of data and using $D_{ph} = \kappa_{ph}/C_{ph}$. It is shown in Fig. 2(c) (left y axis) and reveals three distinct regimes. Above 15 K, D_{ph} decreases with increasing temperature. In the temperature window between 2 and 10 K, D_{ph} displays a maximum and minimum, both strongly dependent on the sample size. Finally, below 1 K, thermal diffusivity becomes sample independent again and continues its enhancement without saturation down to 0.1 K.

In the high-temperature regime, phonon-phonon umklapp collisions set the magnitude of thermal diffusivity. The intermediate-temperature regime is analogous to what is observed in several other solids, including Bi [31] and black phosphorus [10], two other column V elements, and diagnosed as a signature of phonon hydrodynamics [8]. In contrast to those materials, the low-temperature thermal diffusivity of Sb does not become not ballistic but returns to an intrinsic behavior.

The phonon mean-free path can be extracted using the relation $\ell_{ph} = 3D_{ph}/\langle v_s \rangle$, with $\langle v_s \rangle \approx 2900$ m.s^{-1} [32]. ℓ_{ph} remains well below the typical sample size. Figure 3 compares the temperature dependence of ℓ_{ph} in Sb with black phosphorus [10] and Bi [31,33]. Below the hydrodynamic window, phonons in Bi and black P become ballistic: ℓ_{ph} saturates to a value which scales with the crystal size. In the case of Sb, the phononic mean-free path shows no evidence of ballistic transport down to

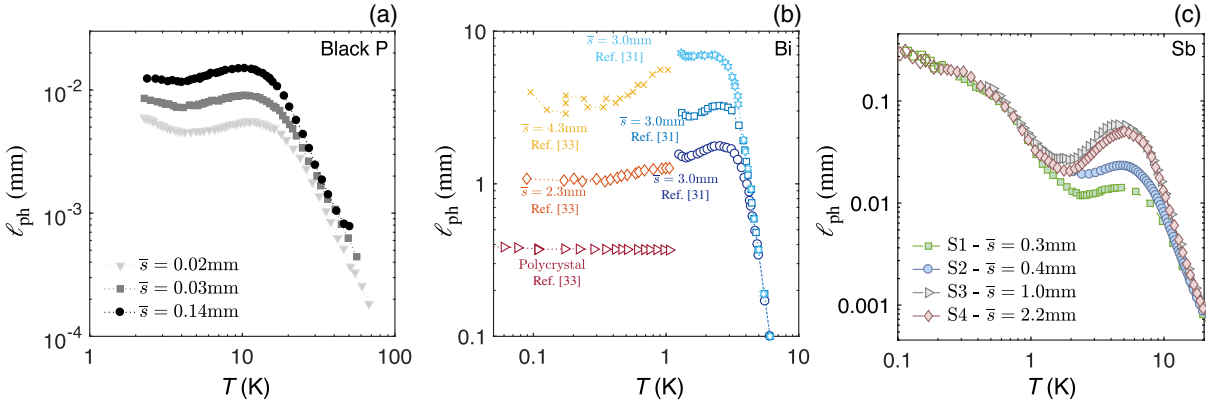

FIG. 3. The phonon mean-free path is short and intrinsic. The temperature dependence of the phonon mean-free path ℓ_{ph} in (a) black phosphorus [10], (b) bismuth [31,33], and (c) antimony (this work) as a function of the temperature. Only in Sb ℓ_{ph} does not evolve with the sample size at low temperature and remains well below the sample thickness.

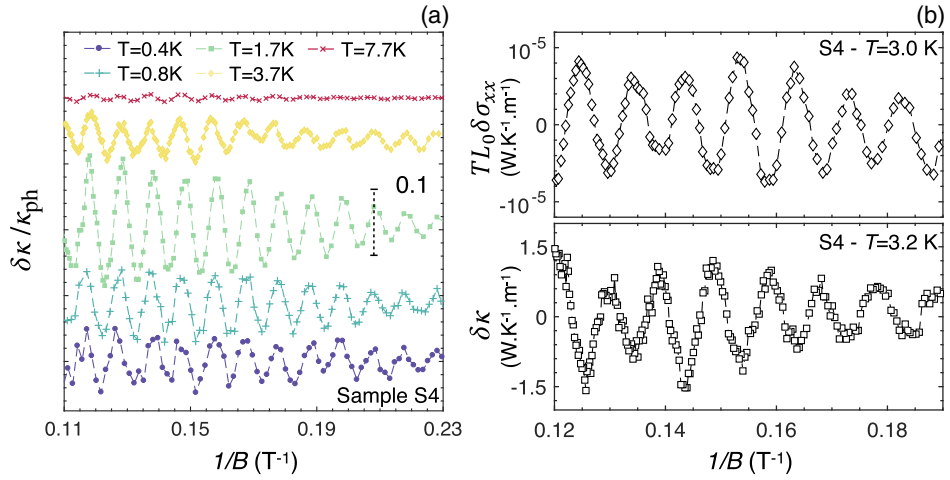

FIG. 4. Quantum oscillations of lattice thermal conductivity. (a) The oscillatory component of the thermal conductivity $\delta\kappa$ is shown (normalized as $\delta\kappa/\kappa_{\rm ph}$) for sample S4 as a function of $1/B$ for various temperatures. Graphs are shifted vertically for clarity. The scale bar corresponds to a relative amplitude of 10%. (b) Comparison of the oscillations observed in the thermal conductivity $\delta\kappa$ and in the electrical conductivity (multiplied by the Sommerfeld value and temperature). Note the 5 orders of magnitude difference in amplitude of oscillations in $TL_0\sigma_{xx}$ and in $\kappa_{\rm ph}$.

$T = 100$ mK and becomes independent of the sample size.

Thus, the phonon mean-free path in antimony is intrinsic below 1 K. The typical wavelength of an acoustic phonon in this temperature range is between 8 and 80 nm. We show below that this intrinsic regime is due to the coupling between acoustic phonons and electronic quasiparticles. In this new intrinsic regime, a typical phonon goes through numerous momentum-exchanging events with electrons before colliding with the boundary of the crystal. Note also the large value of the hydrodynamic correction to the mean-free path which follows from the large ratio of the peak in the Poiseuille regime and the Knudsen minimum [34] in antimony. It becomes as large as 5 in the largest samples, compared to 0.4 in the two other solids. Thin graphite [11] and solid ^{4}He [35] display a hydrodynamic correction comparable to what is found in samples S3 and S4 of this study.

Further evidence for coupling to electrons comes from quantum oscillations of $\kappa_{\rm ph}$ shown in Fig. 4(a). The oscillations, extracted by subtracting a monotonic background, are periodic in $1/B$, and their amplitude depends on the sample size (see Supplemental Material [22]). The extracted frequencies [22] ($f_\alpha = 100$ T and $f_\beta = 350$–380 T) are in good agreement with previous reports for this configuration [36–38]. Quantum oscillations of the thermal conductivity are observed in other semimetals and explained in different manners (see Supplemental Material for details [22]). Here, they can safely be attributed to the phononic component. As seen in Fig. 4(b), their amplitude is 5 orders of magnitude larger than what is expected for any oscillation in the electronic component, given the amplitude of σ_{xx} oscillations. Note that the deviation from the WF law in the hydrodynamic regime, shown in the inset in Fig. 1(c), is much smaller and goes in the opposite way. While the quantum oscillations of thermal conductivity are 10^5 larger than quantum oscillations of electric conductivity, the thermal conductivity in the Poiseuille regime becomes 0.2 times the electric conductivity. In addition, the σ_{xx} and κ_{xx} oscillations are out of phase. This implies that the enhancement of the electronic density of states (caused by the evacuation of a Landau level) pulls down the phononic thermal conductivity, as would happen if phonons were strongly coupled to electrons.

Let us now turn our attention to the electrical properties. Figure 5(a) shows quantum oscillations of the electrical resistivity (the Shubnikov–de Haas effect) in the samples. The Dingle analysis [Fig. 5(b)] yields a mobility μ_D, which is more than 2 orders of magnitude lower than the transport mobility $\mu_{\rm tr}$, extracted from the residual resistivity. A similar observation (that is, $\mu_D \gg \mu_{\rm tr}$) is reported in other dilute metals [39,40]. In the present case, we find that in all the four samples, in spite of the tenfold variation in residual resistivity and $\mu_{\rm tr}$, μ_D is identical. This indicates that $\mu_{\rm tr}$, set by the collision time between momentum-relaxing events, varies from sample to sample. On the other hand, μ_D, set by the broadening of the Landau levels, is intrinsically bound. We see below that this can also fit in our scenario.

The temperature dependence of resistivity provides a crucial piece of information. Its exponent γ ($\rho = \rho_0 + A_\gamma \times T^\gamma$) does *not* show a T^5 behavior at low temperature [inset in Fig. 6(a)]. One can quantify it by taking the logarithmic derivative after subtracting residual resistivity: $\gamma = \{[\partial \ln(\rho - \rho_0)]/(\partial \ln T)\}$. This procedure was previously applied to extract the exponent of resistivity in

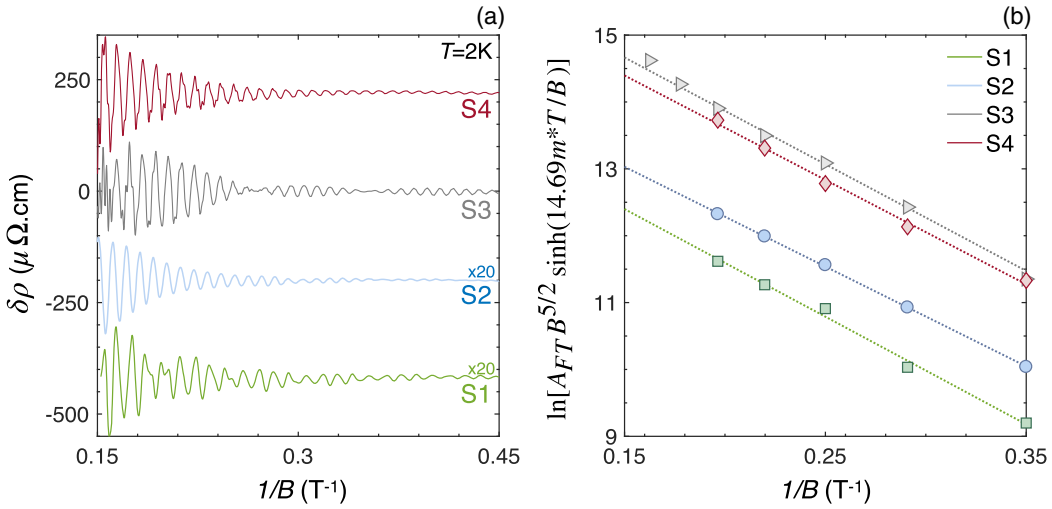

FIG. 5. Invariability of Dingle mobility in contrast to transport mobility. (a) Oscillatory part of the magnetoresistance (for B along the trigonal axis) as a function of $1/B$ at $T = 2$ K in different samples. Curves are shifted vertically and multiplied by a factor 20 for S1 and S2. (b) Dingle analysis of the amplitude A_{FT} of the 100 T peak of the Fourier transform of $\delta\rho$ in the aforementioned sample. In spite of more than one order-of-magnitude difference in residual resistivity, the lines are parallel, indicating no detectable difference in Dingle mobility.

cuprates [41], in heavy fermions [42], and in strontium titanate [43]. The temperature dependence of γ is shown in Fig. 6(a). In the standard (Bloch-Grüneisen) picture of electron-phonon scattering, resistivity is T-linear above the Debye temperature θ_D (or an effective Debye temperature sometimes called the Bloch-Grüneisen temperature) and evolves toward a T^5 behavior upon cooling. Here, $\gamma \approx 1$ indeed at high temperature and increases with decreasing temperature. However, this increase is abruptly interrupted around 15 K [orange arrow in Fig. 6(a)]. Below this temperature, and down to approximately 0.1 K, $\gamma \approx 2$, with no sign of a higher exponent due to phonon scattering.

The same procedure is applied to six Sb samples with different residual resistivities. As seen in Fig. 6(b), all samples show a similar behavior. This observation confirms the intrinsic nature of the abrupt shift to $\gamma \approx 2$ and indicates a suppression of resistive electron-phonon scattering at low temperature. The remaining T^2-dependent resistivity is associated with electron-electron collisions, which scales with the inverse of the Fermi energy (see Supplemental Material [22]).

It is instructive to compare the evolution of the resistivity exponent in Sb with that of other metals. Figure 6(c) shows the temperature dependence of γ in Sb (averaged over all

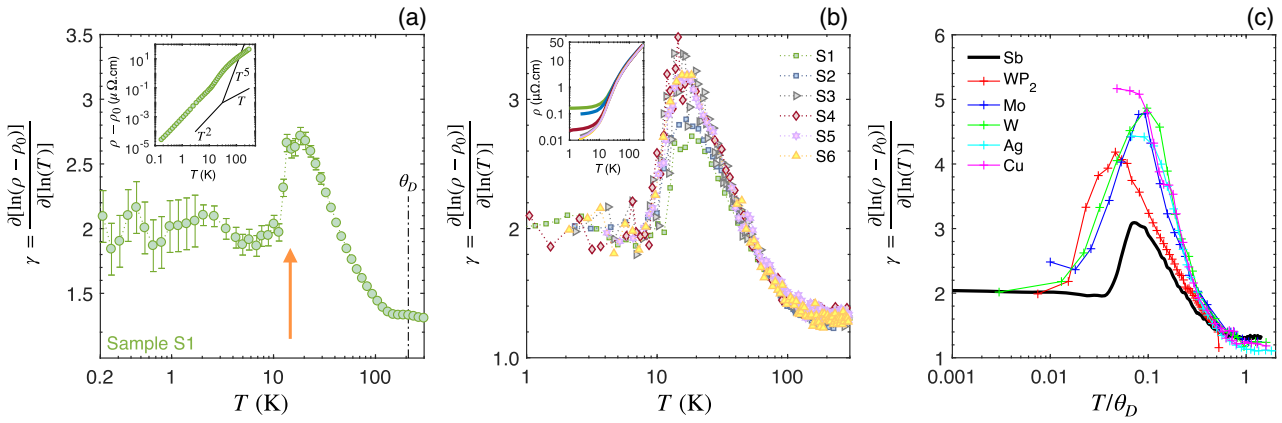

FIG. 6. Resistivity exponent. (a) γ, the exponent of the inelastic resistivity ($\rho = \rho_0 + A_\gamma T^\gamma$), determined from the logarithmic derivative of $\rho - \rho_0$ in sample S1 as a function of the temperature. Error bars represent the 95% confidence bounds. The steady increase in γ is abruptly stopped around $T = 15$ K, marked by an orange arrow. This is the same temperature at which the phonon mean-free path becomes size dependent [arrow in Fig. 2(c)]. (b) The exponent of the inelastic resistivity, γ, in six different Sb samples as a function of the temperature. The inset shows the resistivity of the six samples. (c) Comparison of the temperature dependence of γ in Sb (averaged over the different samples) and five other metals.

six samples) and in five other metals. These are semimetallic WP_2 ($n = p = 2.5 \times 10^{21}$ cm^{-3}) [19], W ($n = p = 2 \times 10^{22}$ cm^{-3}) [44], and Mo ($n = p = 1 \times 10^{22}$ cm^{-3}) [44] as well as noble metals Cu ($n = 8 \times 10^{22}$ cm^{-3}) [45] and Ag ($n = 6 \times 10^{22}$ cm^{-3}) [45]. In almost all cases, when the temperature decreases to one-tenth of the Debye temperature, the exponents increases to 5. This is clearly the case of Ag and Cu. Similar behavior is found in elemental W and Mo. Nevertheless, because of their lower electronic densities, they display a dominant T-square behavior when $T \ll 0.1\Theta_D$. The prefactor of this T-square resistivity is, however, much smaller than in Sb (see Supplemental Material [22]). In contrast to these, the exponent of resistivity in Sb never attains 5 and suddenly drops to 2 around 15 K. A similar but less drastic behavior can be seen in WP_2. The comparison shows that relaxation of the electron momentum via scattering with phonons vanishes most rapidly in Sb. This is not surprising given its lower Fermi energy and smaller Fermi surface.

The sudden interruption of the growth in the exponent of resistivity in Sb is concomitant with the emergence of the hydrodynamic phonon thermal diffusivity [see orange arrows in Figs. 2 and 6(a)]. There is a simple way of linking the two features. Below 15 K, umklapp collisions among phonons become rare, and ph-ph collisions conserve momentum. Therefore, a momentum yielded to a phonon during a collision is not lost to the momentum sink by umklapp. Rather, it eventually returns to the electron bath through another e-ph collision. The only remaining way for electrons to lose momentum is either elastic collisions or inelastic resistive collisions with other electrons, still a significant fraction of e-e collisions [20]. As a consequence, $\gamma \approx 2$, from 10 down to 0.2 K. This interpretation paves the way to explain other remarkable features found in this study, such as the quantum oscillations of the lattice thermal conductivity and the intrinsic nature of the Dingle mobility, and the fact that the phonon and electron scattering time converge at low temperature (see below).

III. DISCUSSION

Usually, phonon hydrodynamics is expected to emerge in a finite temperature window sandwiched between the ballistic and the diffusive regimes [1,8]. In this hydrodynamic window, the shortest timescale is set by the momentum-conserving collisions between phononic quasiparticles. Our case has a twist. As sketched in Fig. 7(a), below $T \approx 15$ K, momentum-conserving collisions between phonons become prominent, but, as the temperature is reduced further, ph-ph scattering is less frequent than electron-phonon scattering ($\tau^N_{\text{ph-ph}} > \tau^N_{\text{ph-}e}$). Below $T \approx 1$ K, the shortest timescale for a phonon corresponds to momentum exchange events with an electron and not with another phonon (or the boundary). In contrast to the common hydrodynamic picture, this new hydrodynamic regime extends down to $T \approx 0.1$ K, instead of being replaced by a ballistic regime.

Figure 7(b) shows the temperature dependence of the typical phonon scattering time. One can distinguish between two subregimes for this e-ph bifluid. Above $T \approx 0.5$ K, the phonon scattering time τ_{ph} increases with cooling following ($\tau_{\text{ph}} \propto T^{-2}$). More specifically, the extracted τ_{ph} is quantitatively close to τ_{e-e}, the typical

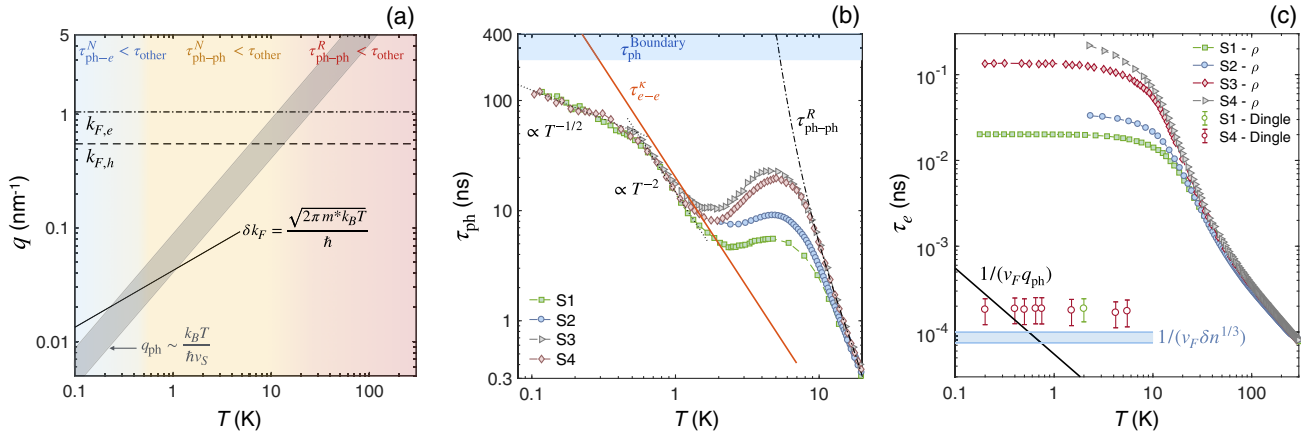

FIG. 7. Hydrodynamic regimes. (a) Evolution of the different wave vectors as a function of T. Three different regions are identified. (b) Temperature dependence of the phonon scattering time extracted from the thermal diffusivity of four samples as a function of T. Above $T \approx 15$ K, momentum-relaxing ph-ph collisions dominate. For $1 < T < 15$ K, momentum-conserving ph-ph collisions lead to a size-dependent decrease in the effective scattering time. Below $T \approx 1$ K, the most frequent events are momentum-conserving e-ph collisions, and the phonon scattering time is close to the e-e scattering time extracted from κ_e. (c) Temperature dependence of the electronic scattering time extracted from the electrical resistivity of four samples alongside the Dingle scattering time for samples S1 and S4. Also shown are the typical time between e-ph collisions (solid black line) and the typical time of electron-defect collisions estimated from the Hall resistivity (see Supplemental Material for details [22]).

time between two momentum-conserving e-e collisions, extracted from the electronic component of the thermal conductivity (discussed in detail in Ref. [20]). The most plausible explanation for this is to assume that at least a sizable fraction of e-e collision events consist in exchanging phonons. Such an idea has been put forward decades ago in other contexts [46,47]. Below $T \approx 0.5$ K, $\tau_{\rm ph}$ saturates toward a $T^{-1/2}$ behavior. This may correspond to a shrinking phase space for an e-ph collision following $\tau^{-1} \propto (q_{\rm ph}/\delta k_F) \propto T^{1/2}$, where $\delta k_F = \sqrt{2\pi m^* k_B T}/\hbar$ is the thermal thickness of the Fermi surface.

Figure 7(c) shows the temperature dependence of the typical electron scattering time, which is much longer than the phonon scattering time. As we see above, the Dingle analysis of quantum oscillations yields another timescale, which is 2–3 orders of magnitude shorter than the transport time and does not vary from one sample to another. Given that thermal and electric transport by electrons yield a quasi-identical scattering time, the difference with the Dingle time cannot be due to the sampling of small-angle collision events. On the other hand, exchanging back and forth a momentum of $\hbar q_p$ with phonons widens the Landau levels by an energy of approximately $\hbar v_F q_{\rm ph}$. As seen in Fig. 7(c), this alternative explanation for the discrepancy between Dingle and transport times gives the right order of magnitude. However, one cannot rule out another possible explanation. Unavoidable point defects (extrinsic atoms), which give rise to the finite Hall resistivity of this compensated metal, can lead to a short Dingle time (see Supplemental Material [22] for details). Introducing controlled disorder is a way to discriminate between the two possibilities.

Thus, the phonon scattering time at cryogenic temperatures is well below the ballistic time and remarkably close to the electron-electron scattering time, which leads us to conclude that the phonon transport time is set by the rate of phonon absorption and emission of colliding electrons.

Note that the formation of such a bifluid does not impede the total thermal conductivity to remain a sum of distinct contributions from electrons and phonons: $\kappa = \kappa_{\rm ph} + \kappa_e$. The first component $\kappa_{\rm ph}$ is insensitive to the magnetic field, but the second $\kappa_e \propto \{[\kappa_e(B=0)]/[1+(\omega_c\tau_e)^2]\}$ is drastically modified by the magnetic field (ω_c is the cyclotron frequency). At zero field, $\kappa_e(B=0) \propto \tau_e$, but in the high-field regime, $\kappa_e(\omega_c\tau_e \gg 1) \propto \tau_e^{-1}$ and becomes negligibly small compared to $\kappa_{\rm ph}$. This feature is what allows us to separate $\kappa_{\rm ph}$ and κ_e. As one can see in Fig. 7(b), at $T \approx 1$ K, $\tau_{\rm ph} \sim \tau_{e-e} \sim 10^{-8}$ s. Meanwhile, at the same temperature, $\tau_e > 2 \times 10^{-11}$ s. Thanks to the lightness of carriers, this ensures that one has $\omega_c\tau_e \gg 1$ at 1 T. Therefore, our picture is quantitatively consistent.

The formation of the bifluid may be traced to the fact that the carrier density in antimony is low enough to host electrons with a long Fermi wavelength yet not sufficiently low to make them irrelevant for scattering phonons. Let us note that the carrier density in antimony is 2 orders of magnitude larger than that of bismuth and 2 orders of magnitude lower than that of WP_2. Therefore, WTe_2, with a carrier density similar to that of antimony, emerges as an interesting platform to investigate the emergence of a similar case of bifluidity.

In summary, we carried out a detailed study of thermal conductivity in antimony samples of different sizes. We found that the phonon mean-free path displays a nonmonotonic temperature dependence, signaling that phononic heat transport in antimony becomes hydrodynamic like bismuth and black phosphorus. In contrast to the latter, however, the phonon mean-free path remains much shorter than the sample size. We argued that this is due to the formation of an electron-phonon bifluid, where electrons frequently transmit and receive phonons. Remarkably, around 1 K, the phonon scattering time and the electron-electron scattering time have the same amplitude and the same temperature dependence.

ACKNOWLEDGMENTS

We thank Yo Machida for discussions. This work was supported by the Agence Nationale de la Recherche (No. ANR-18-CE92-0020-01 and No. ANR-19-CE30-0014-04), by Jeunes Equipes de l'Institut de Physique du Collège de France, and by a grant attributed by the Ile de France regional council. T. L. acknowledges support by the DFG (German Research Foundation) via Project No. LO 818/6-1. The computational resources were provided by Grand Équipment National De Calcul Intensif-Centre Informatique National de l'Enseignement Supérieur (GENCI-CINES) (Grant No. 2020-A0090911099) and the Swiss National Superconducting Center (Grant No. s820).

[1] R. N. Gurzhi, *Hydrodynamic Effects at Low Temperature*, Sov. Phys. Usp. **11**, 255 (1968).

[2] M. J. M. de Jong and L. W. Molenkamp, *Hydrodynamic Electron Flow in High-Mobility Wires*, Phys. Rev. B **51**, 13389 (1995).

[3] P. J. W. Moll, P. Kushwaha, N. Nandi, B. Schmidt, and A. P. Mackenzie, *Evidence for Hydrodynamic Electron Flow in* $PdCoO_2$, Science **351**, 1061 (2016).

[4] J. Crossno, J. K. Shi, K. Wang, X. Liu, A. Harzheim, A. Lucas, S. Sachdev, P. Kim, T. Taniguchi, K. Watanabe *et al.*, *Observation of the Dirac Fluid and the Breakdown of the Wiedemann-Franz Law in Graphene*, Science **351**, 1058 (2016).

[5] D. Bandurin, I. Torre, R. K. Kumar, M. B. Shalom, A. Tomadin, A. Principi, G. Auton, E. Khestanova, K. Novoselov, I. Grigorieva *et al.*, *Negative Local Resistance Caused by Viscous Electron Backflow in Graphene*, Science **351**, 1055 (2016).

[6] J. Gooth, F. Menges, N. Kumar, and V. Süβ, C. Shekhar, Y. Sun, U. Drechsler, R. Zierold, C. Felser, and B. Gotsmann,

Thermal and Electrical Signatures of a Hydrodynamic Electron Fluid in Tungsten Diphosphide, Nat. Commun. **9**, 4093 (2018).

[7] J. A. Sulpizio, L. Ella, A. Rozen, J. Birkbeck, D. J. Perello, D. Dutta, M. Ben-Shalom, T. Taniguchi, K. Watanabe, T. Holder, R. Queiroz, A. Principi, A. Stern, T. Scaffidi, A. K. Geim, and S. Ilani, *Visualizing Poiseuille Flow of Hydrodynamic Electrons*, Nature (London) **576**, 75 (2019).

[8] H. Beck, P. F. Meier, and A. Thellung, *Phonon Hydrodynamics in Solids*, Phys. Status Solidi (a) **24**, 11 (1974).

[9] V. Martelli, J. L. Jiménez, M. Continentino, E. Baggio-Saitovitch, and K. Behnia, *Thermal Transport and Phonon Hydrodynamics in Strontium Titanate*, Phys. Rev. Lett. **120**, 125901 (2018).

[10] Y. Machida, A. Subedi, K. Akiba, A. Miyake, M. Tokunaga, Y. Akahama, K. Izawa, and K. Behnia, *Observation of Poiseuille Flow of Phonons in Black Phosphorus*, Sci. Adv. **4**, eaat3374 (2018).

[11] Y. Machida, N. Matsumoto, T. Isono, and K. Behnia, *Phonon Hydrodynamics and Ultrahigh-Room-Temperature Thermal Conductivity in Thin Graphite*, Science **367**, 309 (2020).

[12] S. A. Hartnoll, P. K. Kovtun, M. Müller, and S. Sachdev, *Theory of the Nernst Effect near Quantum Phase Transitions in Condensed Matter and in Dyonic Black Holes*, Phys. Rev. B **76**, 144502 (2007).

[13] J. Coulter, G. B. Osterhoudt, C. A. C. Garcia, Y. Wang, V. M. Plisson, B. Shen, N. Ni, K. S. Burch, and P. Narang, *Uncovering Electron-Phonon Scattering and Phonon Dynamics in Type-I Weyl Semimetals*, Phys. Rev. B **100**, 220301(R) (2019).

[14] U. Vool, A. Hamo, G. Varnavides, Y. Wang, T. X. Zhou, N. Kumar, Y. Dovzhenko, Z. Qiu, C. A. C. Garcia, A. T. Pierce, J. Gooth, P. Anikeeva, C. Felser, P. Narang, and A. Yacoby, *Imaging Phonon-Mediated Hydrodynamic Flow in* WTe_2, Nat. Phys. **17**, 1216 (2021).

[15] A. Levchenko and J. Schmalian, *Transport Properties of Strongly Coupled Electron-Phonon Liquids*, Ann. Phys. (Amsterdam) **419**, 168218 (2020).

[16] X. Huang and A. Lucas, *Electron-Phonon Hydrodynamics*, Phys. Rev. B **103**, 155128 (2021).

[17] C. Fu, T. Scaffidi, J. Waissman, Y. Sun, R. Saha, S. J. Watzman, A. K. Srivastava, G. Li, W. Schnelle, P. Werner, M. E. Kamminga, S. Sachdev, S. S. P. Parkin, S. A. Hartnoll, C. Felser, and J. Gooth, *Thermoelectric Signatures of the Electron-Phonon Fluid in PtSn4*, arXiv:1802.09468.

[18] C. Herring, *Theory of the Thermoelectric Power of Semiconductors*, Phys. Rev. **96**, 1163 (1954).

[19] A. Jaoui, B. Fauqué, C. W. Rischau, A. Subedi, C. Fu, J. Gooth, N. Kumar, V. Süß, D. L. Maslov, C. Felser, and K. Behnia, *Departure from the Wiedemann-Franz Law in* WP_2 *Driven by Mismatch in T-Square Resistivity Prefactors*, npj Quantum Mater. **3**, 64 (2018).

[20] A. Jaoui, B. Fauqué, and K. Behnia, *Thermal Resistivity and Hydrodynamics of the Degenerate Electron Fluid in Antimony*, Nat. Commun. **12**, 195 (2021).

[21] G. B. Osterhoudt, Y. Wang, C. A. C. Garcia, V. M. Plisson, J. Gooth, C. Felser, P. Narang, and K. S. Burch, *Evidence for Dominant Phonon-Electron Scattering in Weyl Semimetal* WP_2, Phys. Rev. X **11**, 011017 (2021).

[22] See Supplemental Material at http://link.aps.org/supplemental/10.1103/PhysRevX.12.031023 for more details on the samples and measurement methods, details of *ab initio* calculations, quantum oscillations, Dingle mobility, electron-hole compensation, and T-square resistivity prefactor in semimetals.

[23] D. A. Broido, M. Malorny, G. Birner, N. Mingo, and D. A. Stewart, *Intrinsic Lattice Thermal Conductivity of Semiconductors from First Principles*, Appl. Phys. Lett. **91**, 231922 (2007).

[24] L. Lindsay, D. A. Broido, and T. L. Reinecke, *Ab Initio Thermal Transport in Compound Semiconductors*, Phys. Rev. B **87**, 165201 (2013).

[25] T. Shiga, J. Shiomi, J. Ma, O. Delaire, T. Radzynski, A. Lusakowski, K. Esfarjani, and G. Chen, *Microscopic Mechanism of Low Thermal Conductivity in Lead Telluride*, Phys. Rev. B **85**, 155203 (2012).

[26] R. Guo, X. Wang, Y. Kuang, and B. Huang, *First-Principles Study of Anisotropic Thermoelectric Transport Properties of IV-VI Semiconductor Compounds SnSe and SnS*, Phys. Rev. B **92**, 115202 (2015).

[27] B. Dongre, J. Carrete, N. Mingo, and G. K. Madsen, *Ab Initio Lattice Thermal Conductivity of Bulk and Thin-Film* α-Al_2O_3, MRS Commun. **8**, 1119 (2018).

[28] A. Subedi, *First Principles Study of Thermal Conductivity of In* $_2O_3$ *in Relation to* Al_2O_3, Ga_2O_3, *and* $KTaO_3$, arXiv:2101.02664.

[29] G. K. White and S. B. Woods, *The Thermal and Electrical Resistivity of Bismuth and Antimony at Low Temperatures*, Philos. Mag. A **3**, 342 (1958).

[30] H. V. Culbert, *Low-Temperature Specific Heat of Arsenic and Antimony*, Phys. Rev. **157**, 560 (1967).

[31] V. Kopylov and L. Mezhov-Deglin, *Study of Kinetic Coefficients of Bismuth at Helium Temperatures*, Sov. Phys. JETP **65**, 720 (1973).

[32] S. Epstein and A. P. deBretteville, *Elastic Constants of and Wave Propagation in Antimony and Bismuth*, Phys. Rev. **138**, A771 (1965).

[33] W. Pratt and C. Uher, *Thermal Conductivity of Bismuth at Ultralow Temperatures*, Phys. Lett. A **68**, 74 (1978).

[34] M.-D. Pavlovich, *Possibility of Observing a Knudsen Minimum in the Thermal Conductivity of Insulator Crystals*, Sov. Phys. Solid State **22**, 11018 (1980).

[35] L. Mezhov-Deglin, *Measurement of the Thermal Conductivity of Crystalline* ^{4}He, Sov. Phys. JETP **22**, 47 (1966).

[36] L. R. Windmiller, *de Haas–van Alphen Effect and Fermi Surface in Antimony*, Phys. Rev. **149**, 472 (1966).

[37] N. B. Brandt, N. Y. Minina, and C. Chen-Kang, *de Haas–van Alphen Effect in Antimony at Very Low Temperatures*, Sov. Phys. JETP **24**, 73 (1967).

[38] B. Fauqué, X. Yang, W. Tabis, M. Shen, Z. Zhu, C. Proust, Y. Fuseya, and K. Behnia, *Magnetoresistance of Semimetals: The Case of Antimony*, Phys. Rev. Mater. **2**, 114201 (2018).

[39] N. Kumar, Y. Sun, N. Xu, K. Manna, M. Yao, V. Süss, I. Leermakers, O. Young, T. Förster, M. Schmidt, H. Borrmann, B. Yan, U. Zeitler, M. Shi, C. Felser, and C. Shekhar, *Extremely High Magnetoresistance and Conductivity in the Type-II Weyl Semimetals* WP_2 *and* MoP_2, Nat. Commun. **8**, 1642 (2017).

[40] T. Liang, Q. Gibson, M. N. Ali, M. Liu, R. J. Cava, and N. P. Ong, *Ultrahigh Mobility and Giant Magnetoresistance in the Dirac Semimetal* Cd_3As_2, Nat. Mater. **14**, 280 (2015).

[41] R. A. Cooper, Y. Wang, B. Vignolle, O. J. Lipscombe, S. M. Hayden, Y. Tanabe, T. Adachi, Y. Koike, M. Nohara, H. Takagi, C. Proust, and N. E. Hussey, *Anomalous Criticality in the Electrical Resistivity of* $La_{1-x}Sr_xCuO_4$, Science **323**, 603 (2009).

[42] J. Custers, P. Gegenwart, H. Wilhelm, K. Neumaier, Y. Tokiwa, O. Trovarelli, C. Geibel, F. Steglich, C. Pépin, and P. Coleman, *The Break-up of Heavy Electrons at a Quantum Critical Point*, Nature (London) **424**, 524 (2003).

[43] X. Lin, C. W. Rischau, L. Buchauer, A. Jaoui, B. Fauqué, and K. Behnia, *Metallicity without Quasi-particles in Room-Temperature Strontium Titanate*, npj Quantum Mater. **2**, 41 (2017).

[44] P. D. Desai, T. K. Chu, H. M. James, and C. Y. Ho, *Electrical Resistivity of Selected Elements*, J. Phys. Chem. Ref. Data **13**, 1069 (1984).

[45] R. A. Matula, *Electrical Resistivity of Copper, Gold, Palladium, and Silver*, J. Phys. Chem. Ref. Data **8**, 1147 (1979).

[46] A. H. MacDonald, *Electron-Phonon Enhancement of Electron-Electron Scattering in Al*, Phys. Rev. Lett. **44**, 489 (1980).

[47] M. Gurvitch, A. K. Ghosh, H. Lutz, and M. Strongin, *Low-Temperature Resistivity of Ordered and Disordered a*15 *Compounds*, Phys. Rev. B **22**, 128 (1980).